

Article

Feasibility of Recycled Aggregate Concrete in a Novel Anchoring Connection for Beam-to-Concrete-Filled Steel Tube Joints

Jianhua Su ^{1,2}, Qian Zhao ^{1,2}, Li'ao Cai ³, Xiaohui Li ³, Hongyin Pu ³, Wei Dai ³, Jian Zhang ³, Deng Lu ⁴ and Feng Liu ^{3,*}

¹ Guangzhou Research Institute of Construction Industry Co., Ltd., Guangzhou 510520, China

² Guangzhou Construction Engineering Co., Ltd., Guangzhou 510030, China

³ School of Civil and Transportation Engineering, Guangdong University of Technology, Guangzhou 510006, China

⁴ China Construction Third Engineering Bureau Group Co., Ltd., Wuhan 430074, China

* Correspondence: fliu@gdut.edu.cn

Abstract: Owing to the substantial benefits in environmental protection and resource saving, recycled aggregate concrete (RAC) is increasingly used in civil engineering; among the different types, RAC-filled steel tubes are an efficient structural form utilizing the advantages of concrete and steel tubes. This paper proposed a novel full-bolted beam-to-concrete-filled steel tube (CFST) joint and investigated the anchoring behavior of the steel plates embedded in RAC-filled steel tubes, which represents the behavior of the tensile zone in this joint, to demonstrate the feasibility of utilizing RAC in composite structures. The specimen consisted of a CFST and a connecting plate embedded in the CFST. In total, 18 specimens were tested to study the effects of concrete type (i.e., recycled aggregate concrete and natural aggregate concrete), anchoring type (i.e., plate with holes, notches, and rebars), and plate thickness on the pullout behavior, such as anchorage strength, load–displacement response, and ductility. Based on experimental results, the aggregate type of the concrete does not affect the pullout behavior obviously but the influence of anchoring type is significant. Among the three anchoring methods, the plate with rebars exhibits the best performance in terms of anchorage strength and ductility, and is recommended for the beam-to-CFST joint. In addition, plate thickness obviously affects the behavior of plates with holes and notches, the bearing area of which is proportional to the thickness, whereas the pullout behavior of the plates with rebars is independent of thickness. Finally, design formulas are proposed to estimate the anchorage strength of the connecting plates, and their reasonability is validated using the experimental results.

Keywords: recycled aggregate concrete; anchoring behavior; pullout test; connecting plates; load–displacement response; theoretical model



Citation: Su, J.; Zhao, Q.; Cai, L.; Li, X.; Pu, H.; Dai, W.; Zhang, J.; Lu, D.; Liu, F. Feasibility of Recycled Aggregate Concrete in a Novel Anchoring Connection for Beam-to-Concrete-Filled Steel Tube Joints. *Buildings* **2024**, *14*, 1178. <https://doi.org/10.3390/buildings14041178>

Academic Editor: Flavio Stochino

Received: 30 March 2024

Revised: 16 April 2024

Accepted: 18 April 2024

Published: 21 April 2024



Copyright: © 2024 by the authors. Licensee MDPI, Basel, Switzerland. This article is an open access article distributed under the terms and conditions of the Creative Commons Attribution (CC BY) license (<https://creativecommons.org/licenses/by/4.0/>).

1. Introduction

With rapid urbanization, lots of infrastructures are demolished worldwide, resulting in a huge amount of construction waste. This had led to severe impacts on the environment and sustainability [1–7]. To solve this issue, we proposed using crushed waste concrete as the coarse aggregate of concrete, named recycled aggregate concrete (RAC) [8–10]. The utilization of RAC efficiently reduces waste concrete, which mitigates the environment impacts, and solves the resource shortage problem in the construction industry. Currently, extensive experimental and theoretical studies have been conducted on the mechanical properties and mixture design of RAC, as well as on the structural behavior of RAC members and structures [11–14]. In general, the mechanical properties of RAC are somewhat less superior to those of natural aggregate concrete (NAC), but the carbon footprint embedded in RAC is much lower than that of NAC [15,16]. It was found that the replacement ratio of recycled aggregate is the critical parameter that affects the behavior of RAC. As the replacement ratio increases, the mechanical properties of RAC tend to decrease [17,18].

The RAC-filled steel tube is a commonly used structural form in practice, and could utilize the advantages of both steel and concrete [19,20]. The steel tube could provide confinements to RAC to increase the strength and ductility of the concrete [21,22]. Furthermore, the local buckling of steel tube could be postponed or avoided by the in-filled concrete, resulting in an enhancement of the steel tube's local buckling capacity. The RAC-filled steel tube has the advantages of high strength, high ductility, and high energy dissipation capacity [23–26]. Currently, the commonly used type for the I section beam-to-square concrete-filled steel tube (CFST) column connection include joints with interior diaphragms, exterior diaphragms, and through diaphragms, hybrid joints with welds and bolts, joints with vertical stiffeners, and joints with binding bars [27–30]. These joints involve on-site welding, which may increase the construction period and affect the quality of welds. In addition, welds in joints are prone to brittle failure during earthquakes. Therefore, full-bolted-joints are encouraged for beam-to-column connections to improve the performance of the connections.

This study proposed a new type of I beam-to-CFST joint that is fully bolted. As shown in Figure 1, there are three connecting plates, and one end of each is embedded in CFST while the other end is bolted to the flanges and the web of the I-beam. Different measures could be adopted to increase the anchorage of the connecting plates, such as setting steel bars, and cutting holes or notches in the plates. Specially, the configuration of connecting plates with steel bars is similar to that of perfobond rib connectors (PBLs), in which the shear resistance comes from the bearing of the end concrete, the shear of the concrete dowel, and the shear of the rebar [31–33]. Nevertheless, PBL is used in steel–concrete composite beams to maintain the bond between the concrete slab and the steel beam. The anchoring behavior of connecting plates in CFST is different from that of PBLs. In addition, it is more difficult to set rebars in a position for close sections than it is to set them in composite beams. Therefore, it is worthwhile to explore other efficient methods to improve the anchorage of the connection plates in CFSTs and investigate the anchoring behavior for the proposal of design methods.

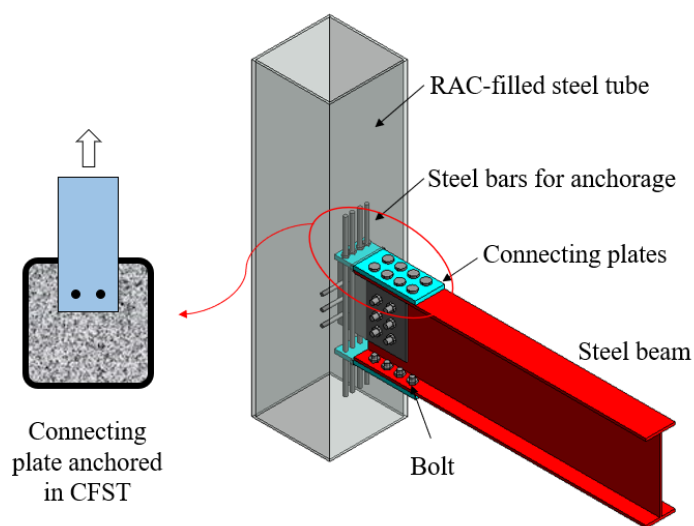


Figure 1. A novel full-bolted beam-to-CFST joint.

Although there are no studies for the proposed configurations, the anchorage behavior of blind bolts in CFSTs have been extensively investigated via pullout tests and may provide some insights for this study. Various types of blind bolts were studied, such as Extended Hollo Bolt [34], T-bolt [35], and the Ajax anchored bolt [36]. By setting anchors, the anchorage strength could be greatly enhanced and the pullout capacity comes mainly from the anchorage of the bolt's anchor and the bearing of the tube face wall [37]. The anchorage strength depends on the embedment depth of the anchor, the bearing area of anchor-to-concrete, and the strength of the concrete. It is noted that this study focused on

the anchorage of a steel plate, which is different from bolts with anchors, and the anchorage mechanism is also different.

This study focused on the anchoring behavior of steel plates embedded in square RAC/NAC-filled steel tubes using pullout tests. Three types of anchoring methods, namely plates with circular holes, plates with rectangular notches, and plates with rebars, were proposed and investigated. In total, 18 specimens were tested to investigate the effects of the key parameters, including the replacement ratio of RAC, thickness of the plates, and anchoring methods, on the pullout behavior (e.g., ultimate capacity, load–displacement curves, and ductility). Thereafter, theoretical studies were conducted and formulas were proposed to estimate the ultimate pullout capacities (i.e., the anchorage strength) of the steel plates anchored in the RAC-filled steel tubes.

2. Experimental Program

2.1. Specimens

Pullout specimens were adopted to investigate the tensile behavior of the tension zone of the beam-to-column joint. In total, 18 specimens were tested under monotonic pullout loads. The parameters investigated in this study include the concrete type (i.e., normal concrete and RAC), the thickness of the connecting plate (i.e., 6 mm and 10 mm), and the anchoring type (i.e., the plate with holes, plate with notches, and plate with rebars).

The specimen consisted of a 650 mm long RAC (or NAC)-filled steel tube (CFST) and a 120 mm by 280 mm connecting plate anchored in the CFST. Dimensions of the specimen are shown in Figure 2, in which T is the plate thickness and the embedment depth of the plate is 80 mm. The dimensions of the CFST are 200 mm \times 650 mm \times 8 mm. Details of the anchoring type are shown in Figure 3, where A1, A2, B1, B2, and C indicate the anchorage type. The size of the rectangular slot on the top surface of the CFST is 122 mm by $T + 2$ mm, where T is the thickness of the connecting plate.

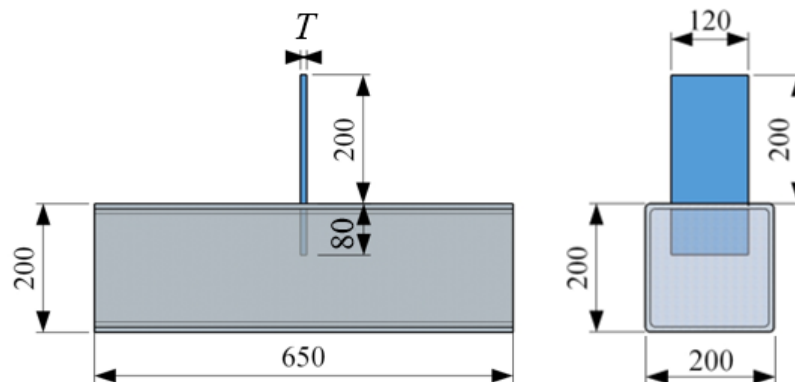


Figure 2. Dimensions of the pullout specimen.

Details of all the tested specimens are listed in Table 1. The label of the specimen consists of the anchorage configuration (A1, A2, B1, B2, and C, as illustrated in Figure 3), rebar diameter (“r” followed by the nominal diameter in mm for a type C specimen), tube thickness (“T” followed by the nominal thickness in mm), and RA replacement ratio (“F” followed by the replacement percentage). For example, C-r8-T6-F100 means that the pullout specimen has a 6 mm thick connecting plate with 8 mm diameter rebars, and the RA replacement ratio is 100%.

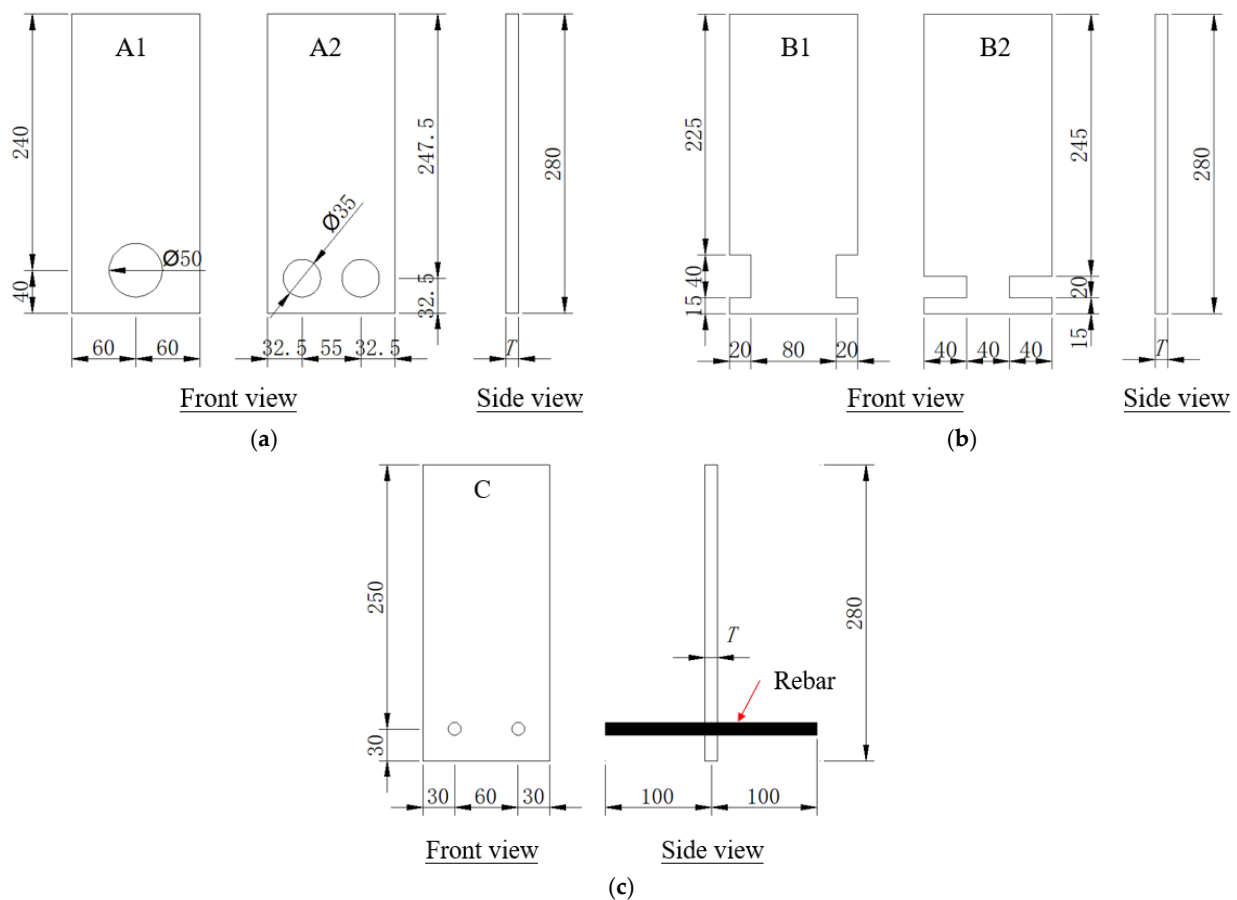


Figure 3. Details of the connecting plates with (a) holes; (b) notches; (c) steel bars.

Table 1. Specimen table.

Specimen	Configuration	T (mm)	RA Replacement (%)	Remark
A1-T6-F100	1 Φ 50 hole	6	100	With holes
A1-T10-F100	1 Φ 50 hole	10	100	
A1-T10-F0	1 Φ 50 hole	10	0	
A2-T6-F100	2 Φ 35 hole	6	100	
A2-T10-F100	2 Φ 35 hole	10	100	
A2-T10-F0	2 Φ 35 hole	10	0	
B1-T6-F100	2 \square 20 \times 40 notch	6	100	With notches
B1-T10-F100	2 \square 20 \times 40 notch	10	100	
B1-T10-F0	2 \square 20 \times 40 notch	10	0	
B2-T6-F100	2 \square 40 \times 20 notch	6	100	
B2-T10-F100	2 \square 40 \times 20 notch	10	100	
B2-T10-F0	2 \square 40 \times 20 notch	10	0	
C-r8-T6-F100	2 Φ 8 rebar	6	100	With rebars
C-r8-T10-F100	2 Φ 8 rebar	10	100	
C-r8-T10-F0	2 Φ 8 rebar	10	0	
C-r12-T6-F100	2 Φ 12 rebar	6	100	
C-r12-T10-F100	2 Φ 12 rebar	10	100	
C-r12-T10-F0	2 Φ 12 rebar	10	0	

The manufacturing procedure of the pullout specimens is as follows: (1) fix the hollow tube on the timber plate with silicon; (2) position the connecting plate and rebars (if applicable) with temporary supports; (3) cast the concrete. Figure 4 shows the pictures of the steel tubes, connecting plates, and specimens before we casted the concrete and

casted the specimens. Six concrete cylinders with a diameter of 150 mm and height of 300 mm were also casted to measure the concrete strength. After casting the concrete, all the specimens and cylinders were cured at ambient temperature until the testing date. The actual curing time of the specimens was 28~32 days.

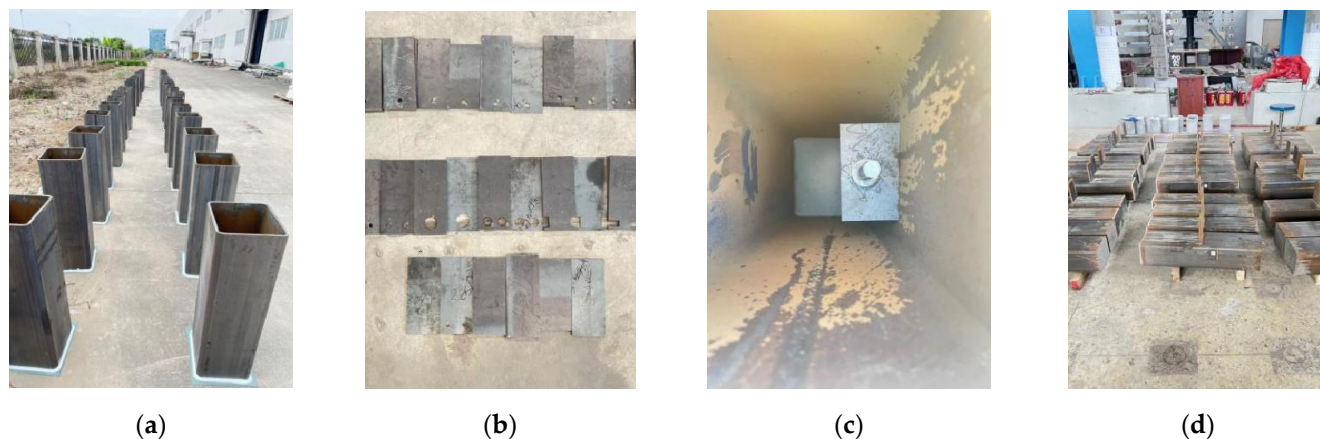


Figure 4. Preparation of pullout specimens: (a) steel tubes; (b) connecting plates; (c) specimen before casting concrete; (d) casted specimens.

2.2. Materials

The designed grade of the concrete is C50 with a water-to-cement ratio of 0.55, and the mixture is shown in Table 2. Both recycled aggregate concrete (RAC) and natural aggregate concrete (NAC) were adopted in this study. The recycled aggregate (RA) was obtained from the demolished concrete of old buildings. The old concrete was crushed into small sizes, screened, washed, and dried (Figure 5a). The mechanical and physical properties of the RA met the requirements in [38]. The NA was fabricated from crushed basalt (Figure 5b). Both RA and NA had continued particle size distributions with a size range of 5–20 mm, which met the requirement indicated in GB/T 25177-2010 [39]. River sand was adopted as the fine aggregate. General-purpose cement (Grade 42.5) was used as the binder, and its initial and final setting time were >45 min and <10 h, respectively. A polycarboxylate-based water reducer was used for the concrete to improve workability. At the time of the specimen test, a compressive test was conducted on the concrete cylinders with a diameter of 150 mm and height of 300 mm to measure the compressive strength (f_c') and Young's modulus (E_c'); the average measured values are listed in Table 2. The compressive strengths of RAC and NAC are very close. The main reason is that the RA was crushed from concrete with granite as coarse aggregate, whereas the coarse aggregate for NAC was basalt, the strength and hardness of which are lower than those of granite. In addition, RA has higher water absorption than NA does, resulting in a lower water-to-cement ratio for RAC. Therefore, strength reduction was not observed after replacing NA with RA.

Table 2. Mixture and hardened properties of concrete.

Replacement Ratio of RA (%)	Mass per Unit Volume (kg/m^3)						f_c' (MPa)	E_c' (GPa)
	Cement	Sand	Natural CA	Recycled CA	Water	Water Reducer		
0%	425	762	1018	0	175.5	8.5	50.3	49.4
100%	425	762	0	1018	175.5	8.5	49.3	41.5

Note: CA = coarse aggregate.

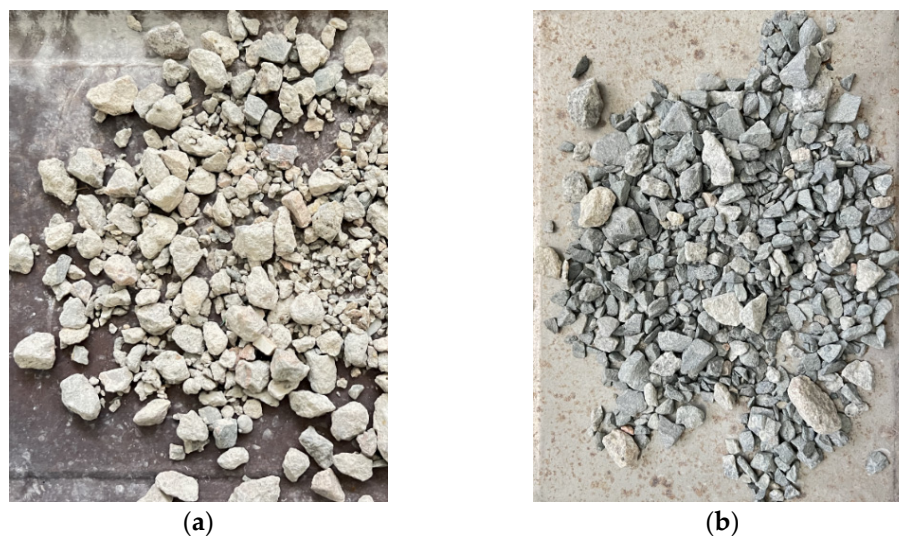


Figure 5. Coarse aggregates: (a) RA; (b) NA.

The square steel tubes were cold-formed and purchased from the market. Both the square steel tube and connecting plates were made of Q235 steel, the nominal yield strength of which is 235 MPa. The grade of the deformed steel rebars was HRB400 (nominal yield strength = 400 MPa). Tensile coupon tests were conducted on the steel plates and rebars, and the measured material properties are listed in Table 3. It is necessary to mention that the properties of the steel tube were not measured experimentally, as past similar studies [37,40] indicated that the yield strength of a steel tube is not a governing parameter affecting the anchorage of steel plates.

Table 3. Material properties of steel plates and rebars.

Type	E_s (GPa)	f_y (MPa)	f_u (MPa)
Steel plate	211	328	444
Steel rebar	209	453	672

2.3. Experimental Setup

Figure 6 shows the experimental setup for the pullout test. The connecting plate was gripped by the 500 kN universal testing machine (MTS-322), and the load was applied upward. Two 500 mm long welded rectangular hollow tubes (130 mm × 150 mm × 30 mm) were placed on the CFST, working as the reaction beams to resist the upward movement of the specimen. Each reaction beam was connected to the base plate of the test machine via two high-strength steel (HSS) rods measuring a diameter of 28 mm. The clear distance between the reaction beams was about 350 mm, ensuring that the constraining effect at beam ends did not affect the pullout behavior of the specimen. The load was applied under displacement control with a loading rate of 1.2 mm/min. The experiment was terminated when obvious failure occurred, such as when the pullout of the steel plate, the fracture of the steel plate, or a substantial drop in the applied load was observed.

Two linear variable displacement transducers (LVDTs) were deployed between the actuator and the top surface of the CFST (near the edge) to measure the vertical displacement of the connecting plate (Figure 6). It is necessary to mention that the average value of LVDTs was the same as that for the displacement recorded by the test machine. Seven strain gauges (S1, S2, S3, S4, S5, S6 and S7) were fixed on the top surface of CFST, as shown in Figure 7, to measure the strain distribution of the steel tube. All the data, such as load, displacements, and strains, were recorded simultaneously during the experiment.

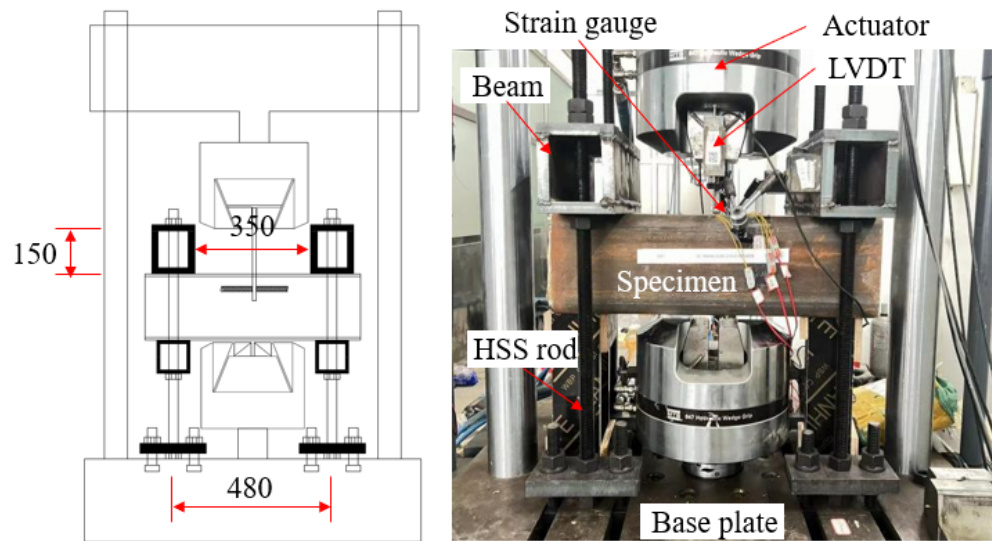


Figure 6. Experimental setup for pullout test.

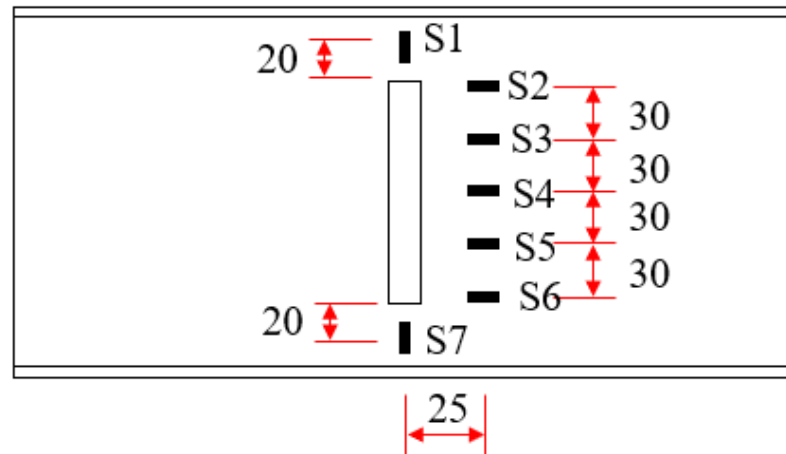


Figure 7. Layout of strain gauges.

3. Experimental Results

3.1. Failure Modes

The deformed shapes of the tested specimens are presented in Figure 8. After each test, the CFSTs were cut off and the concrete was removed to observe the failure modes of the connecting plates, as shown in Figure 8. In general, owing to the different anchorage mechanisms, the failure modes of the tested specimens (plates with holes, notches, and rebars) varied significantly.

As shown in Figure 8a, the deformation of the steel tube was insignificant during the test, indicating that only a small portion of concrete was involved in resisting the applied force. Furthermore, the bearing deformation of the steel plate was not obvious. Localized failure happened in the concrete within the holes. This was likely due to the shear failure and bearing failure (concrete-to-steel) of the concrete. For specimens with notches (Figure 8b), the deformation of the CFST was not obvious. However, significant deformation was observed in steel plate's notches. The bottom edge of the notch could be regarded as a cantilever beam in contact with the filled concrete. As shown in Figure 8b, with the increase in notch width (from 20 mm to 40 mm), the governing failure mode of the notch edge changed from shearing-governed to bending-governed due to the increase in the length-to-depth ratio of the cantilever beam. Excessive deformation of CFST face wall was observed for specimens with rebars (Figure 8c). Shear failure of the rebars occurred for the plates with thickness of 10 mm. A combination of the shear and bending failure

of rebars and the tearing of the steel plate was observed for the 6 mm thick plate. The deformation of the rebar was mainly induced by the shear and bending effects, which could be regarded as a beam on continuous springs (i.e., surrounded concrete) and it is under laterally distributed loads. Su et al. [41] and He et al. [42] observed the similar failure mode and defined it as the tension-shear failure.

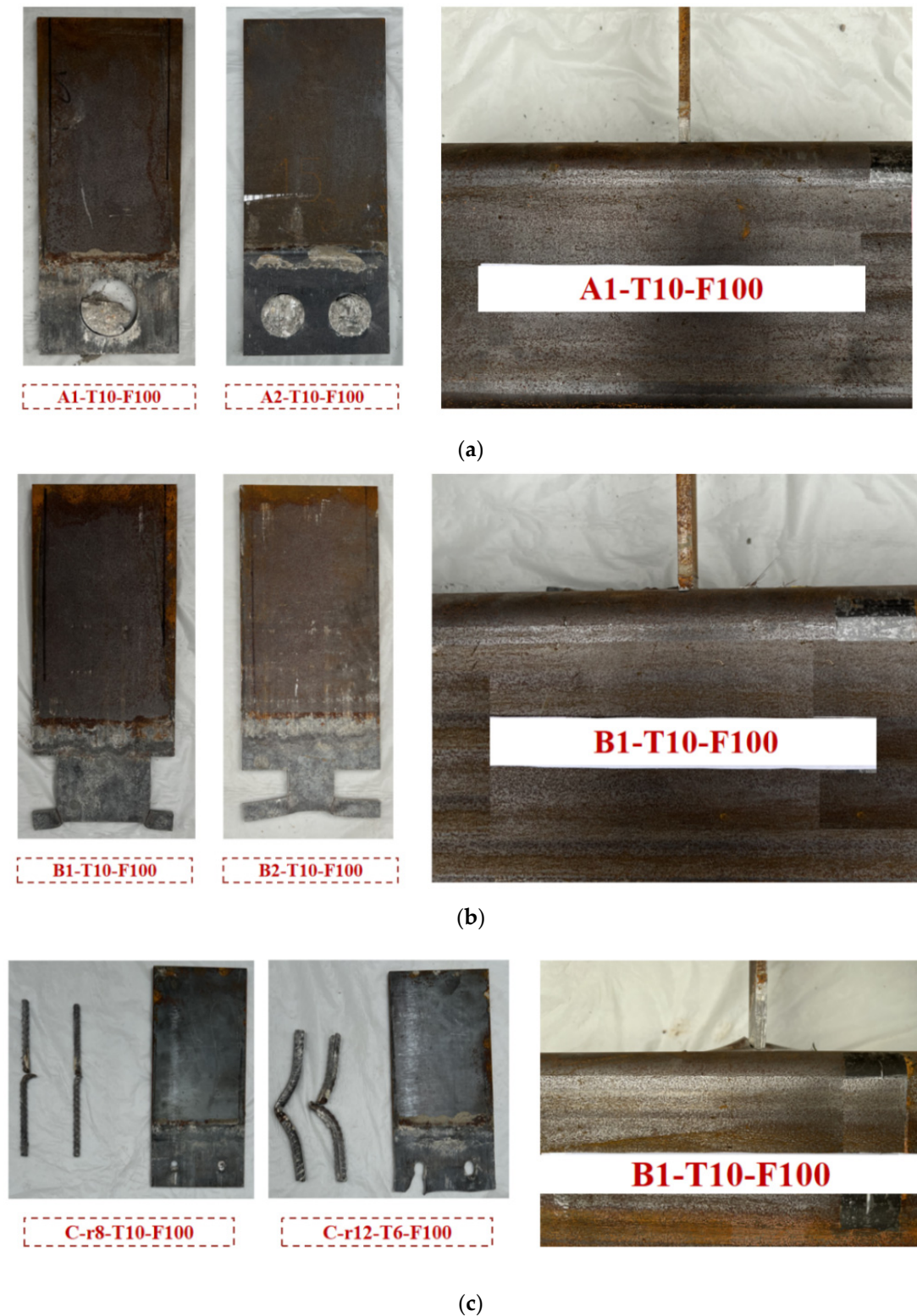


Figure 8. Failure modes: (a) plate with holes; (b) plate with notches; (c) plate with rebars.

3.2. Load–Displacement Curves

Load–displacement curves of all the tested specimens are shown in Figure 9, in which the vertical displacement was recorded by the test machine. In general, the peak load and the shapes of the curves varies greatly depending on the anchoring methods and configurations.

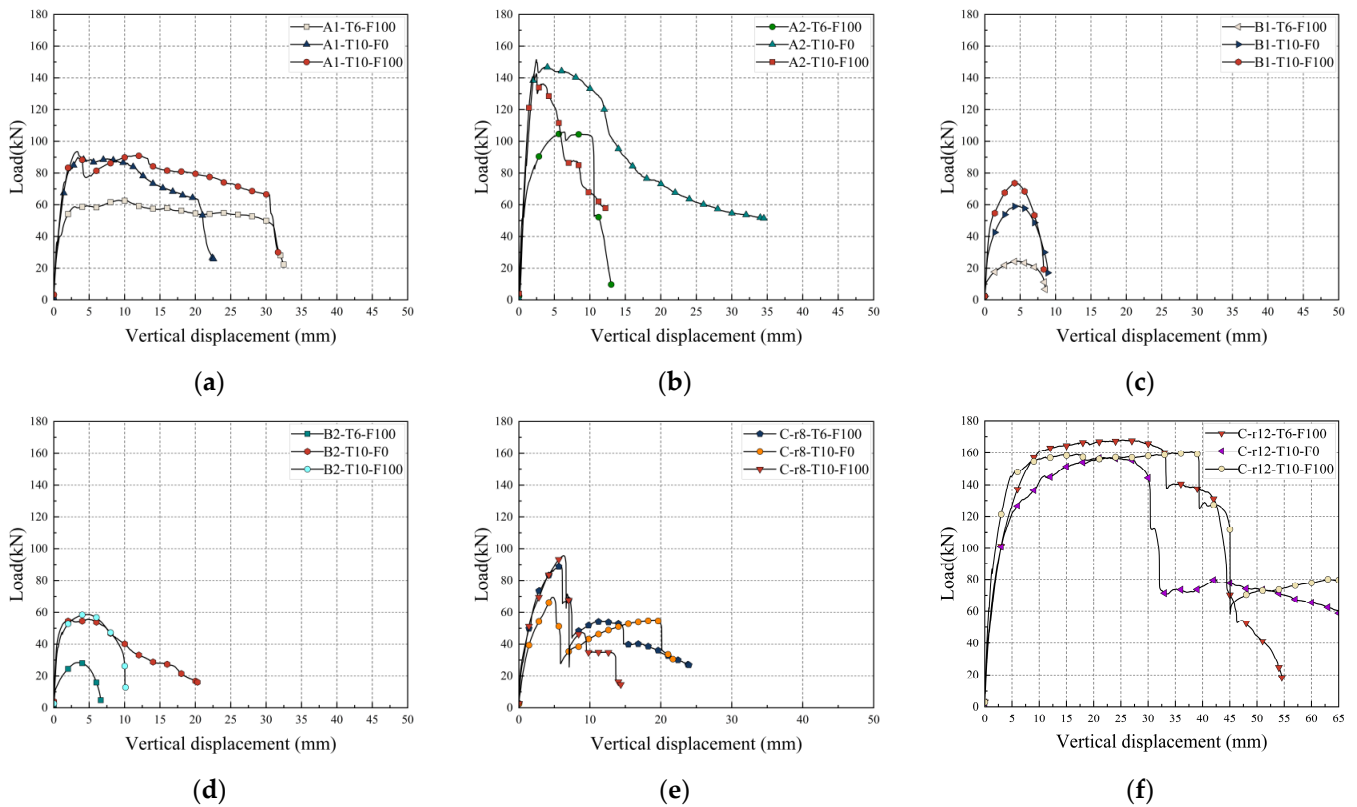


Figure 9. Load–displacement curves of tested specimens. (a) Plates with one hole (A1), (b) plates with two holes (A2), (c) plates with B1-type notches, (d) plates with B2-type notches, (e) plates with 8 mm diameter bars, (f) plates with 12 mm diameter bars.

For connecting plates with holes, the anchorage strength increases by about 50% if the thickness is increased from 6 mm to 10 mm (Figure 9a). Although the total void areas are the same, plates with one $\Phi 50$ hole have a lower anchorage strength than those with two $\Phi 35$ holes (Figure 9b), which is due to the larger bearing area of the latter. After reaching the peak load, plates with one hole (A1) can sustain the applied load without an obvious load drop, indicating that this configuration (with one larger hole) has better ductility than the A2 configuration (with two smaller holes). The reason is that the bearing deformation in the A1 plate is more significant than that in the A2 plate and that the bearing failure is usually more ductile than the shear failure of the concrete cylinder within the hole. For the plates with holes, the bearing area is proportional to the hole diameter whereas the shear area is proportional to the square of hole diameter. By decreasing the diameter (e.g., from 50 mm to 35 mm), the failure mode may change from bearing-dominated to shear-dominated, and the latter failure will be more brittle. Effects of concrete type (NAC vs. RAC) on the anchorage strength and curve shape are not obvious, except that specimen A2-T10-F100 shows a faster load drop after the peak load than its natural aggregate counterpart does. In addition, the displacements corresponding to the anchorage strength are about 2–4 mm, confirming the experimental observation that the deformation of CFST was not obvious.

Figure 9c,d show the load–displacement curves of the plates with notch dimensions (width \times height) of 20 mm \times 40 mm (B1) and 40 mm \times 20 mm (B2), respectively. As expected, concrete type does not influence the pullout behavior obviously. Nevertheless,

the plate thickness greatly affects the anchorage strength as the bearing area is proportional to the thickness. In general, effects of the notch dimensions on the peak load are not obvious whereas the B2 group shows a slightly slower load drop than that of the B1 group.

For plates with rebars (Figure 9e,f), the effects of plate thickness and concrete type on the pullout behavior are insignificant. Nevertheless, the anchorage strength and ductility are greatly enhanced by an increase in the rebar diameter from 8 mm to 12 mm, which is caused by the increase in the bearing area in concrete. After a dramatic load drop, a strength re-gain is observed for the plates with $\Phi 6$ rebars (Figure 9e). In general, specimens with $\Phi 12$ rebars exhibit the best performance among the tested specimens.

3.3. Key Experimental Results

Based on the load–displacement curves, key experimental results, including the yield capacity (P_y), ultimate capacity (P_u), displacement at P_y (Δ_y), displacement at P_u (Δ_u), and ductility index (DI) could be determined. The P_u , also called anchorage strength in this study, is the peak load of the load–displacement curve. As there is no obvious yielding plateau of the load–displacement curves, the method in [43] was adopted to specify the P_y and Δ_y . As illustrated in Figure 10, the procedures for determining P_y are as follow: (1) draw the line OA, the slope of which is the initial stiffness; (2) draw a vertical line at A to obtain intersection B; (3) draw the line OB and find intersection C; (4) draw a vertical line at C to obtain the yield point D (Δ_y, P_y). In this paper, the ductility index is defined as the ratio of the area covered by the load–displacement curve of OBDEF to OBD (Figure 10), in which the load at F is equal to $0.8P_u$. All the values of $P_u, P_y, \Delta_u, \Delta_y$, and DI are summarized in Table 4 and will be used for the discussions in Section 4.

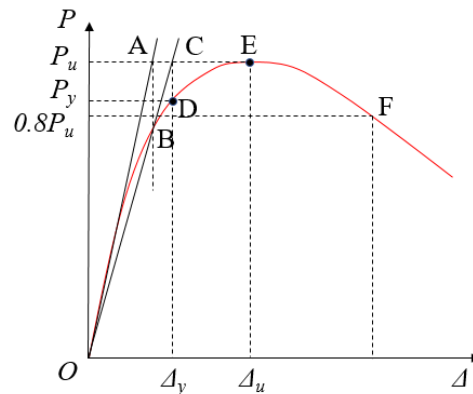


Figure 10. Determination of the yield point and the ductility index.

Table 4. Experimental results and predictions.

Specimen	P_y (kN)	Δ_y (mm)	P_u (kN)	Δ_u (mm)	DI	N_p (kN)	N_p/P_u
A1-T6-F100	36.4	1.14	62.6	9.3	82.5	60.6	1.03
A1-T10-F100	54.5	1.57	93.6	3.3	45.2	101.0	1.08
A1-T10-F0	70.4	1.51	89.8	3.4	22.3	103.2	1.15
A2-T6-F100	62.3	1.56	105.9	6.4	20.1	84.8	0.80
A2-T10-F100	102.4	1.53	142.7	2.5	8.0	141.4	0.99
A2-T10-F0	109.8	2.01	151.5	2.5	14.0	144.4	0.95
B1-T6-F100	11.7	0.67	24.4	4.4	38.8	28.0	1.15
B1-T10-F100	48.0	1.29	73.8	4.4	13.0	60.3	0.82
B1-T10-F0	31.6	1.15	59.2	4.6	19.5	61.6	1.04
B2-T6-F100	12.6	0.76	28.4	3.6	25.8	28.0	0.99
B2-T10-F100	37.2	0.85	58.7	4.3	26.4	60.3	1.03
B2-T10-F0	36.3	0.55	55.7	4.8	43.9	61.6	1.11
C-r8-T6-F100	58.0	1.80	89.4	5.9	7.9	71.9	0.80
C-r8-T10-F100	63.6	2.27	95.6	6.3	6.4	71.9	0.75
C-r8-T10-F0	26.9	2.02	69.4	4.8	9.4	72.0	1.04
C-r12-T6-F100	110.1	3.58	168.0	25.2	31.1	160.0	0.95
C-r12-T10-F100	110.8	3.64	160.4	38.0	30.1	160.0	1.00
C-r12-T10-F0	107.6	5.10	157.0	21.8	15.2	160.1	1.02

3.4. Strain Distributions of CFST

The strain distributions on the CFST's face wall of the specimens with RAC and a plate thickness of 10 mm are shown in Figure 11, which includes the strain data corresponding to the loads of $0.2P_u$, $0.4P_u$, $0.6P_u$, and $0.8P_u$ before reaching the peak load. The layout of the strain gauges is illustrated in Figure 7. The strains in the corner (S2 and S6) are positive (in tension), whereas the strains in other locations (S1, S3~S5, and S7) are negative (in compression). The strain data were mainly used for assessing the deformation of the CFST and verifying the finite element models that will be constructed in a future study.

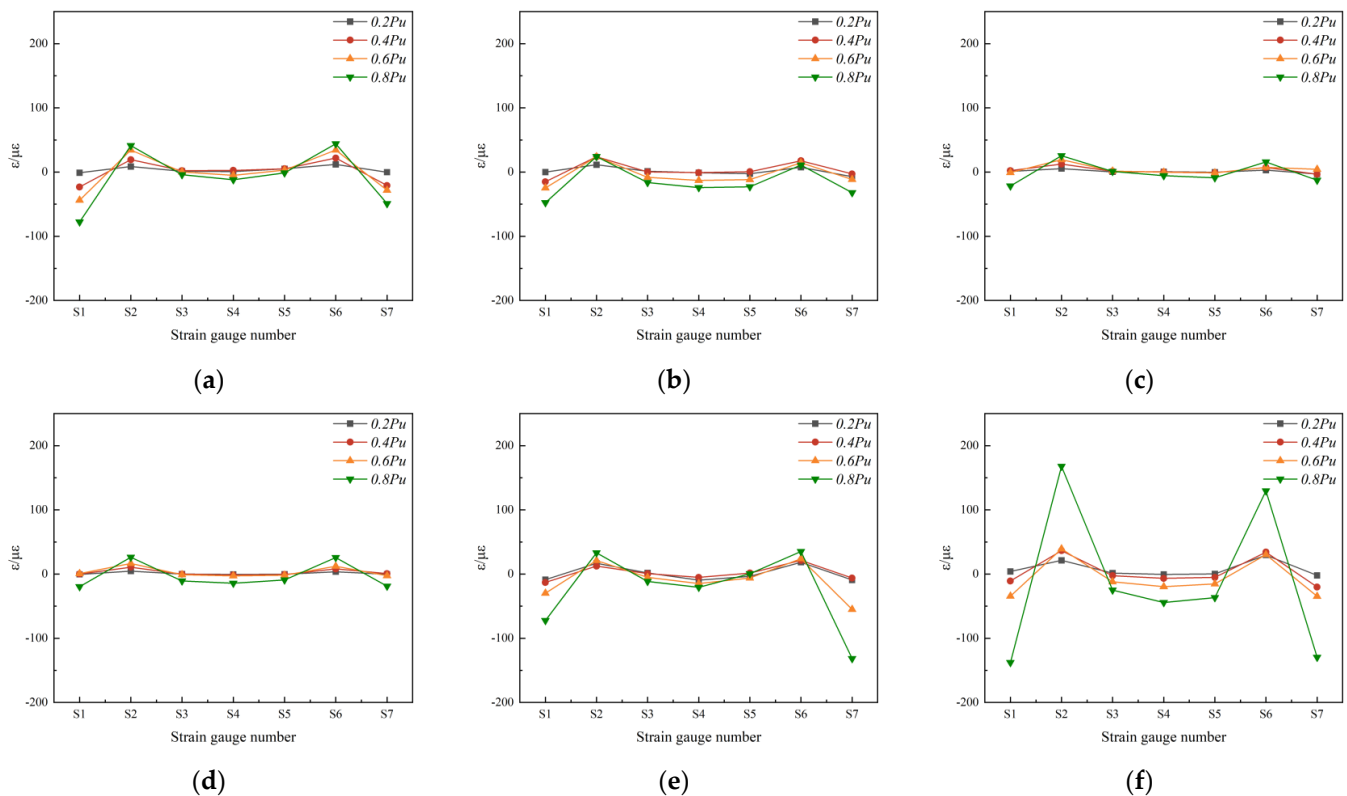


Figure 11. Strain distributions. (a) A1-T10-F100, (b) A2-T10-F100, (c) B1-T10-F100, (d) B2-T10-F100, (e) C-r8-T10-F100, and (f) C-r12-T10-F100.

As shown in Figure 11, the absolute strain values are quite small, and are less than $50 \mu\epsilon$, except for specimen C-r12-T10-F100, indicating that the deformation of the steel tube was negligible. It can be concluded that the deformation of the connecting plate and the CFST can be ignored during service load. Furthermore, in the determination of the initial stiffness of a beam-to-column joint carried out by using the well-known component method, the stiffness of CFST and connecting plates could be assumed as infinity. A higher value of the strain indicates larger deformation of the tube face wall, and this was induced by the expansion and movement of the in-filled concrete. Therefore, more concrete was involved in anchoring the connecting plates if the strains were larger. As shown in Figure 11, specimen C-r12-T10-F100 has the most concrete involved and would have the highest anchorage strength, which is in agreement with the experimental results in Table 4. Plates with holes and notches had a lower anchorage strength as only a small portion of concrete could participate in resisting the applied load. In addition, the strain in the middle (SG4) was larger than the strains in the locations near the side walls (i.e., SG3 and SG5). This phenomenon could be explained by simplifying the tube face wall as a fixed supported beam (i.e., larger strain at mid-span).

4. Discussions

4.1. Effect of Anchoring Type and Configurations

The effects of the key parameters, such as concrete type, anchoring type, anchoring configurations (e.g., size and number of holes, direction of notches, and diameter of rebars), and plate thickness on the pullout behavior of the connecting plate are discussed in this section. The pullout behavior mainly includes the anchorage strength, load–displacement response, and ductility index, which were defined in Figure 10.

As shown in Table 4 and Figure 9, the anchoring type (hole, notch or rebar) has a significant effect on the anchorage strength, ductility index, and pullout load–displacement curves, owing to the different anchorage mechanisms. The plates with rebars or holes had much higher anchorage strength than plates with notches did. For plates with similar total void areas, the configuration of smaller holes led to a higher anchorage strength (by about 70%) but lower ductility. With the same notch area, the effect of notch direction (see Figure 3b) on the anchorage strength was not obvious. The plate with wider notches exhibited slightly better ductility (i.e., a slower load drop and a higher ductility index) than that with narrow notches. By increasing the diameter of the rebars, the anchorage strength and ductility were greatly improved. The connecting plates with $\Phi 12$ rebars performed the best among the tested specimens. Therefore, the anchoring type of using a rebar is recommended for the connecting plates in beam-to-column joints. Nevertheless, it is necessary to mention that the construction of this configuration is less convenient than that of connecting plates with holes or notches.

4.2. Effect of Plate Thickness

As shown in Table 4 and Figure 12, the anchorage strength of the 10 mm thick connecting plates with holes is 35~50% larger than that of the 6 mm thick plates, whereas the enhancement is 100~170% for the plates with notches. Plate thickness has a significant impact on anchorage strength as the anchorage strength is mainly contributed by the bearing effect, the bearing area of which depends on the plate thickness. Nevertheless, the ductility index shows a decreasing trend (about 50%) with the increase in plate thickness. For plates with rebars, the effects of thickness on the pullout behavior are not obvious. The reason is that the applied load is mainly resisted by the bearing of the rebars, which is not related to the plate thickness.

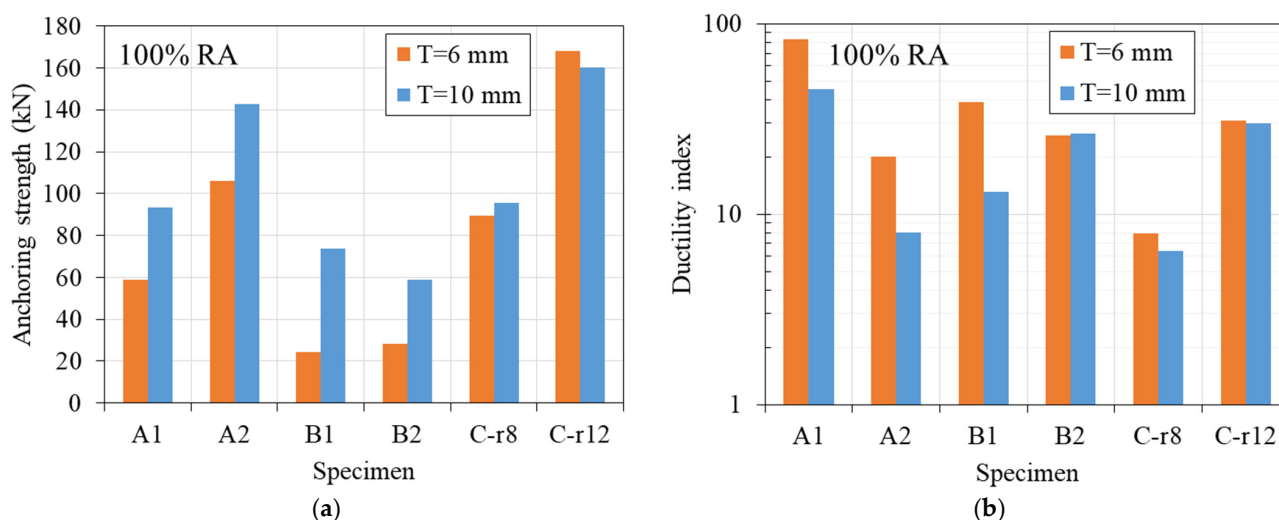


Figure 12. Effect of plate thickness on the pullout behavior. (a) Anchorage strength and (b) ductility index.

4.3. Effect of Concrete Type

One of the aims of this study was to investigate whether or not recycled aggregate has an obvious effect on the anchoring behavior of plates. As reported in Section 2.2, with

the same mix proportions, RAC has a similar compressive strength but slightly lower Young's modulus compared with NAC, probably because of the lower modulus of recycled aggregates than that of natural aggregates. As shown in Figures 9 and 13, the effects of the RA content on the anchorage strengths, and load–displacement curves are insignificant. NAC specimens showed slightly higher ductility than RAC specimens did, as shown in Figure 13b, likely due to the higher modulus of NAC. Nevertheless, this observation is only valid for four of the six groups (i.e., A2, B1, B2, and C-r6) and more research is needed. Therefore, it could be concluded that RAC has similar anchorage behavior to that of NAC, provided that the compressive strengths are similar.

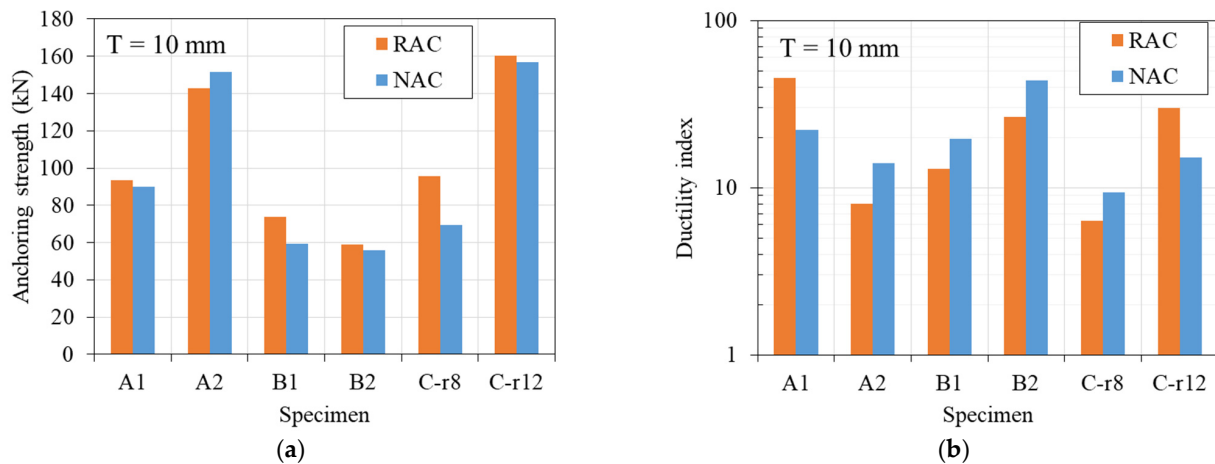


Figure 13. Effect of concrete type on the pullout behavior: (a) Anchorage strength and (b) ductility index.

5. Prediction for the Anchorage Strength of the Connecting Plate

5.1. Connecting Plate with Holes

The possible failure modes of the connecting plates with holes are the bearing failure of the hole, the shear failure of the concrete cylinder within the hole, and the bearing failure of the concrete within the hole. The anchorage strength (N_p) is the lower strength of the bearing strength of steel (N_{bs}), shear strength of concrete (N_{sc}), and bearing strength of concrete (N_{bc}).

$$N_p = \min(N_{bs}, N_{sc}, N_{bc}) \quad (1)$$

Based on the design methods for bolted connections, Equation (2) from GB50017 [44] was adopted to predict the bearing strength of the steel plate:

$$N_{bs} = n d_h t f_{bs} \quad (2)$$

where N_{bs} is the bearing strength of steel plate, d_h is the diameter of the hole, n is the number of the holes, t is the thickness of the plate, and f_{bs} is the bearing strength of the steel plate, taking this as 405 MPa for Q235 steel [39] or considering it equal to $0.67(f_y + f_u)$, as suggested by the HK code [45], where f_y and f_u are the yield strength and ultimate strength, respectively.

The current design method for determining the shear strength of a perfobond rib connector in JTG [46] is adopted to calculate the shear strength of concrete within the holes (N_{sc}):

$$N_{sc} = 1.4 d_h^2 f'_c \quad (3)$$

where f'_c is the compressive strength of concrete.

As indicated by the experimental observations, the failure mode of the tested specimens is the localized bearing failure of the concrete within the hole. Equation (4) is proposed to estimate the bearing strength of the concrete:

$$N_{bc} = \eta n d_h t f'_c \quad (4)$$

where f'_c is the compressive strength of concrete, and η is an empirical coefficient accounting for the bearing strength enhancement of the localized concrete induced by confinement. The value for η is obtained from the regression analysis of the experimental data, and it is recommended to be 4.1. Therefore, the anchorage strength could then be determined via Equation (1).

5.2. Connecting Plate with Notches

By analyzing the bearing stress in the notch, Equation (5) is proposed to predict the anchorage strength of the plate with notches:

$$N_p = \chi n b_n t f'_c \quad (5)$$

where n is the number of notches, b_n is the width of the notch, t is the plate thickness, f'_c is the concrete compressive strength, and χ is an empirical coefficient that considers the effect of notch size on anchorage strength.

Based on the experimental results, there are several important findings regarding the anchorage strength and failure modes: (1) the anchorage strength is not proportional to the thickness of the plate; (2) Although the bearing areas are the same, the anchorage strength differs somewhat for different notch widths (b_n); (3) the failure of the connecting plate can be regarded as a combination of the bearing failure of concrete and the bending failure of the cantilever deep beam with a cross-section of h_n by t_n and a length of b_n (Figure 14). Therefore, χ is assumed to be related to the size of the notch, and governs the bending and shear behavior of the notch. Via regression analysis, as shown in Figure 15, Equation (6) is proposed to estimate the value of χ :

$$\chi = \frac{5}{\sqrt{b_n^2 / (h_n t)}} \quad (6)$$

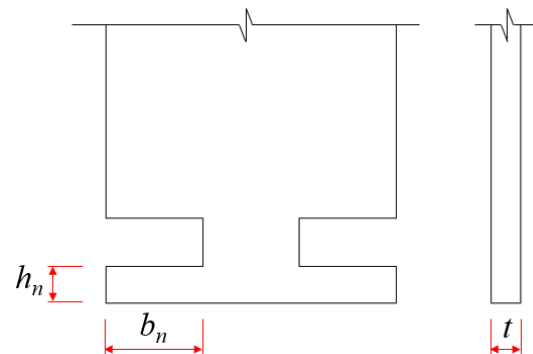


Figure 14. Dimensions of the notch.

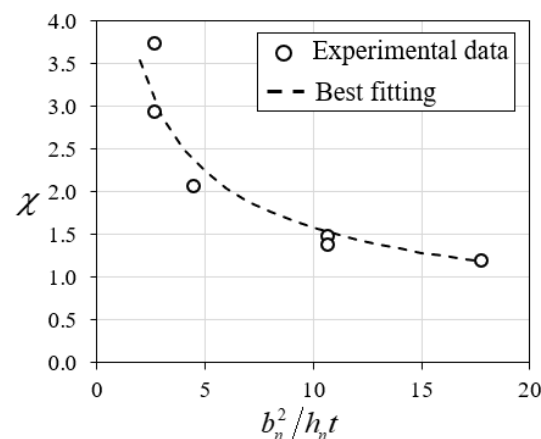


Figure 15. Determination of the empirical coefficient, χ , in Equation (5).

5.3. Connecting Plate with Rebars

The experimental results indicated that the anchoring mechanism of the plate with rebars is similar to that of perfobond rib connectors in resisting shear load. The anchorage strength is proposed to be estimated via the existing design method for perfobond rib connectors in JTG [46]:

$$N_p = 1.4n(d_h^2 - d_s^2)f'_c + 1.2nd_s^2f_y \quad (7)$$

where n is the number of rebars, d_h is the diameter of the hole, d_s is the diameter of the rebar, f'_c is the compressive strength of the concrete, and f_y is the yield strength of the rebar.

5.4. Verifications

A comparison of the experimental and predicted anchorage strengths of the tested specimens is summarized in Table 4 and Figure 16. The average experimental-to-predicted ratios are 1.00, 1.02, and 0.93, whereas the COVs (coefficient of variations) are 0.11, 0.10, and 0.12, for the connecting plates with holes, notches, and rebars, respectively. Therefore, the proposed methods could reasonably estimate the anchorage strength. Nevertheless, it is necessary to mention that the coefficients in Equations (4) and (6) are determined by regressing the experimental data of this study. If more data are available in the future, those formulas could be further refined. The prediction of JTG [46] on the anchorage strength of the steel plate with rebars is conservative. The main reason would be that the concrete in this study is confined by the square steel tube but the confinement effect does not exist in perfobond rib connectors.

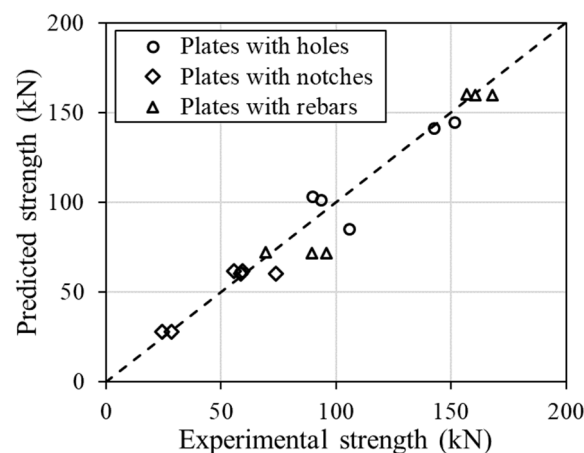


Figure 16. Comparison of the experimental and predicted anchorage strengths.

6. Conclusions

This paper presents an experimental and theoretical study on the pullout behavior of connecting plates embedded in recycled/natural aggregate concrete-filled square tubes (CFSTs), which could simulate the behavior of the tension zone in a novel full-bolted steel beam-to-CFST joint. Effects of the recycled aggregate replacement, anchoring type, and plate thickness on the pullout behavior (e.g., anchorage strength, load–displacement curves, and ductility) are discussed. Theoretical models are then proposed to estimate the anchorage strength of the connecting plates. The following conclusions could be drawn:

- (1) Mechanical properties of recycled aggregate concrete are similar to those of natural aggregate concrete with the same mixtures. Using recycled aggregate for a CFST does not obviously affect the pullout behavior of plates, demonstrating the feasibility of using RAC for composite structures.
- (2) The failure modes of the specimens greatly depend on the anchoring types and configurations. Plates with rebars exhibit higher strength and ductility than the plates with holes or notches, so it is a recommended anchoring method for beam-to-CFST joints.

- (3) With the same void area, plates with two small holes have higher strength than plates with one large hole do, likely due to the increase in bearing area. The effect of the notch dimension (20 mm × 40 mm vs. 40 mm × 20 mm, same area but different direction) on the anchorage strength is not significant, whereas the ductility is slightly influenced. The diameter of the rebars greatly affects the anchorage strength and ductility of the connecting plates.
- (4) Because the bearing area is proportional to the plate thickness, thickness has a significant influence on the pullout behavior of the connecting plates with holes and notches. However, the behavior of the plates with rebars is not affected by the plate thickness.
- (5) Deformations of the connecting plate and CFST are negligible, and their stiffness could be assumed to be infinity in the determination of the initial stiffness of a beam-to-column joint using the component method.
- (6) The proposed formulas could reasonably predict the anchorage strength of the connecting plates with holes and notches. The current method for perfo-bond rib connectors somewhat underestimates the anchorage strength of the connecting plates with rebars, likely due to the lack of consideration of the confining effect in CFSTs, which is a major difference compared with that in perfo-bond rib connectors.

Author Contributions: Conceptualization, J.S. and Q.Z.; methodology, J.S.; software, J.Z.; validation, X.L. and D.L.; investigation, L.C., H.P. and W.D.; resources, Q.Z. and D.L.; writing—original draft, L.C.; writing—review and editing, X.L.; visualization, H.P., W.D. and J.Z.; software, J.Z.; Supervision, F.L.; project administration, F.L.; funding acquisition, J.S. and F.L. All authors have read and agreed to the published version of the manuscript.

Funding: The authors gratefully acknowledge the financial support provided by the Special Foundation for Assembly Construction of Guangzhou Construction Engineering Co., Ltd. ([2019]-KJ002), the National Natural Science Foundation of China (12072080).

Data Availability Statement: The original contributions presented in the study are included in the article, further inquiries can be directed to the corresponding authors.

Conflicts of Interest: Authors Jianhua Su and Qian Zhao were employed by the company Guangzhou Research Institute of Construction Industry Co., Ltd. Authors Jianhua Su and Qian Zhao were employed by the company Guangzhou Construction Engineering Co., Ltd. Author Deng Lu was employed by the company China Construction Third Engineering Bureau Group Co., Ltd. The remaining authors declare that the research was conducted in the absence of any commercial or financial relationships that could be construed as a potential conflict of interest.

References

1. Lai, Y.-Y.; Yeh, L.-H.; Chen, P.-F.; Sung, P.-H.; Lee, Y.-M. Management and Recycling of Construction Waste in Taiwan. *Procedia Environ. Sci.* **2016**, *35*, 723–730. [[CrossRef](#)]
2. Zhen, H.; Xiong, Z.; Song, Y.; Li, L.; Qiu, Y.; Zou, X.; Chen, B.; Chen, D.; Liu, F.; Ji, Y. Early mechanical performance of glass fibre-reinforced manufactured sand concrete. *J. Build. Eng.* **2024**, *83*, 108440. [[CrossRef](#)]
3. Zhu, H.; Xiong, Z.; Song, Y.; Zhou, K.; Su, Y. Effect of Expansion Agent and Glass Fiber on the Dynamic Splitting Tensile Properties of Seawater–Sea-Sand Concrete. *Buildings* **2024**, *14*, 217. [[CrossRef](#)]
4. Lin, J.-X.; Luo, R.-H.; Su, J.-Y.; Guo, Y.-C.; Chen, W.-S. Coarse synthetic fibers (PP and POM) as a replacement to steel fibers in UHPC: Tensile behavior, environmental and economic assessment. *Constr. Build. Mater.* **2024**, *412*, 134654. [[CrossRef](#)]
5. Chen, Z.; Yu, J.; Nong, Y.; Yang, Y.; Zhang, H.; Tang, Y. Beyond time: Enhancing corrosion resistance of geopolymer concrete and BFRP bars in seawater. *Compos. Struct.* **2023**, *322*, 117439. [[CrossRef](#)]
6. Pan, Z.; Liu, F.; Li, H.; Li, X.; Wang, D.; Ling, Z.; Zhu, H.; Zhu, Y. Performance Evaluation of Thermal Insulation Rubberized Mortar Modified by Fly Ash and Glass Fiber. *Buildings* **2024**, *14*, 221. [[CrossRef](#)]
7. Xiong, Z.; Mai, G.; Pan, Z.; Chen, Z.; Jian, J.; Wang, D.; Ling, Z.; Li, L. Synergistic effect of expansive agents and glass fibres on fatigue bending performance of seawater sea sand concrete. *Constr. Build. Mater.* **2024**, *421*, 135665. [[CrossRef](#)]
8. Ding, T.; Xiao, J.; Tam, V.W.Y. A closed-loop life cycle assessment of recycled aggregate concrete utilization in China. *Waste Manag.* **2016**, *56*, 367–375. [[CrossRef](#)] [[PubMed](#)]
9. Chen, X.; Xiao, X.; Wu, Q.; Cheng, Z.; Xu, X.; Cheng, S.; Zhao, R. Effect of magnesium phosphate cement on the mechanical properties and microstructure of recycled aggregate and recycled aggregate concrete. *J. Build. Eng.* **2021**, *46*, 103611. [[CrossRef](#)]

10. Superti, V.; Houmani, C.; Hansmann, R.; Baur, I.; Binder, C.R. Strategies for a Circular Economy in the Construction and Demolition Sector: Identifying the Factors Affecting the Recommendation of Recycled Concrete. *Sustainability* **2021**, *13*, 4113. [[CrossRef](#)]
11. Zhang, X.; Kuang, X.; Wang, F.; Wang, S. Strength indices and conversion relations for basalt fiber-reinforced recycled aggregate concrete. *Dyna-Bilbao* **2019**, *94*, 82–87. [[CrossRef](#)]
12. Kurda, R.; de Brito, J.; Silvestre, J.D. Combined influence of recycled concrete aggregates and high contents of fly ash on concrete properties. *Constr. Build. Mater.* **2017**, *157*, 554–572. [[CrossRef](#)]
13. Papavasileiou, G.S.; Charmpis, D.C. Earthquake-resistant buildings with steel or composite columns: Comparative assessment using structural optimization. *J. Build. Eng.* **2020**, *27*, 100988. [[CrossRef](#)]
14. Ma, H.; Liu, F.; Wu, Y.; Xin, X.; Zhao, Y. Axial compression tests and numerical simulation of steel reinforced recycled concrete short columns confined by carbon fiber reinforced plastics strips. *Front. Struct. Civ. Eng.* **2022**, *16*, 817–842. [[CrossRef](#)]
15. Duan, Z.; Li, B.; Xiao, J.; Guo, W. Optimizing mix proportion of recycled aggregate concrete by readjusting the aggregate gradation. *Struct. Concr.* **2020**, *22*, E22–E32. [[CrossRef](#)]
16. Liang, C.; Liu, T.; Xiao, J.; Zou, D.; Yang, Q. Effect of Stress Amplitude on the Damping of Recycled Aggregate Concrete. *Materials* **2015**, *8*, 5298–5312. [[CrossRef](#)]
17. Wang, Y.; Deng, Z.; Xiao, J.; Li, T.; Li, J. Mechanical properties of recycled aggregate concrete under compression-shear stress state. *Constr. Build. Mater.* **2021**, *271*, 121894. [[CrossRef](#)]
18. Xiao, J.; Zhang, K.; Akbarnezhad, A. Variability of stress-strain relationship for recycled aggregate concrete under uniaxial compression loading. *J. Clean. Prod.* **2018**, *181*, 753–771. [[CrossRef](#)]
19. Tam, V.W.Y.; Xiao, J.; Liu, S.; Chen, Z. Behaviors of recycled aggregate concrete-filled steel tubular columns under eccentric loadings. *Front. Struct. Civ. Eng.* **2018**, *13*, 628–639. [[CrossRef](#)]
20. Yang, Y.-F.; Han, L.-H.; Zhu, L.-T. Experimental Performance of Recycled Aggregate Concrete-Filled Circular Steel Tubular Columns Subjected to Cyclic Flexural Loadings. *Adv. Struct. Eng.* **2009**, *12*, 183–194. [[CrossRef](#)]
21. Ma, H.; Xue, J.; Zhang, X.; Luo, D. Seismic performance of steel-reinforced recycled concrete columns under low cyclic loads. *Constr. Build. Mater.* **2013**, *48*, 229–237. [[CrossRef](#)]
22. Ma, H.; Xue, J.; Liu, Y.; Dong, J. Numerical analysis and horizontal bearing capacity of steel reinforced recycled concrete columns. *Steel Compos. Struct.* **2016**, *22*, 797–820. [[CrossRef](#)]
23. Ma, H.; Qiang, J.; Xi, J.; Zhao, Y. Cyclic loading tests and horizontal bearing capacity of recycled concrete filled circular steel tube and profile steel composite columns. *J. Constr. Steel Res.* **2022**, *199*, 107572. [[CrossRef](#)]
24. Zhang, W.-H.; Wang, R.; Zhao, H.; Lam, D.; Chen, P. Axial-load response of CFST stub columns with external stainless steel and recycled aggregate concrete: Testing, mechanism analysis and design. *Eng. Struct.* **2022**, *256*, 113968. [[CrossRef](#)]
25. Lyu, W.-Q.; Han, L.-H. Investigation on bond strength between recycled aggregate concrete (RAC) and steel tube in RAC-filled steel tubes. *J. Constr. Steel Res.* **2019**, *155*, 438–459. [[CrossRef](#)]
26. Zhao, H.; Zhang, W.-H.; Wang, R.; Hou, C.-C.; Lam, D. Axial compression behaviour of round-ended recycled aggregate concrete-filled steel tube stub columns (RE-RACFST): Experiment, numerical modeling and design. *Eng. Struct.* **2023**, *276*, 115376. [[CrossRef](#)]
27. Choi, S.-M.; Park, S.-H.; Yun, Y.-S.; Kim, J.-H. A study on the seismic performance of concrete-filled square steel tube column-to-beam connections reinforced with asymmetric lower diaphragms. *J. Constr. Steel Res.* **2010**, *66*, 962–970. [[CrossRef](#)]
28. Qin, Y.; Chen, Z.; Wang, X. Experimental investigation of new internal-diaphragm connections to CFT columns under cyclic loading. *J. Constr. Steel Res.* **2014**, *98*, 35–44. [[CrossRef](#)]
29. Qin, Y.; Chen, Z.; Wang, X. Elastoplastic behavior of through-diaphragm connections to concrete-filled rectangular steel tubular columns. *J. Constr. Steel Res.* **2014**, *93*, 88–96. [[CrossRef](#)]
30. Yang, J.; Sheehan, T.; Dai, X.; Lam, D. Experimental study of beam to concrete-filled elliptical steel tubular column connections. *Thin-Walled Struct.* **2015**, *95*, 16–23. [[CrossRef](#)]
31. Vianna, J.d.C.; de Andrade, S.; Vellasco, P.d.S.; Costa-Neves, L. Experimental study of Perfobond shear connectors in composite construction. *J. Constr. Steel Res.* **2013**, *81*, 62–75. [[CrossRef](#)]
32. Fang, Z.; Wu, J.; Xian, B.; Zhao, G.; Fang, S.; Jiang, H.; Ma, Y. Shear Performance and Design Recommendations of Single Embedded Nut Bolted Shear Connectors in Prefabricated Steel-UHPC Composite Beams. *Steel Compos. Struct.* **2024**, *50*, 319–336.
33. Fang, Z.; Wu, J.; Xu, X.; Ma, Y.; Fang, S.; Zhao, G.; Jiang, H. Grouped rubber-sleeved studs-UHPC pocket connections in prefabricated steel-UHPC composite beams: Shear performance under monotonic and cyclic loadings. *Eng. Struct.* **2024**, *305*, 117781. [[CrossRef](#)]
34. Tizani, W.; Cabrera, M.; Mahmood, M.; Ninic, J.; Wang, F. The behaviour of anchored extended blind bolts in concrete-filled tubes. *Steel Constr.* **2022**, *15*, 51–58. [[CrossRef](#)]
35. Ng, W.H.; Kong, S.Y.; Chua, Y.S.; Bai, Y. Tensile behaviour of innovative one-sided bolts in concrete-filled steel tubular connections. *J. Constr. Steel Res.* **2022**, *191*, 107165. [[CrossRef](#)]
36. Yao, H.; Goldsworthy, H.; Gad, E. Experimental and numerical investigation of the tensile behavior of blind-bolted T-stub connections to concrete-filled circular columns. *J. Struct. Eng.* **2008**, *134*, 198–208. [[CrossRef](#)]
37. Li, Y.; Chan, T.; Zhao, X. Review on blind bolted connections to concrete-filled steel tubes. *Thin-Walled Struct.* **2023**, *183*, 110444. [[CrossRef](#)]

38. GB 175; Common Portland Cement. China Standards Press: Beijing, China, 2020. (In Chinese)
39. GB/T25177; Recycled Coarse Aggregate for Concrete. China Construction Industry Press: Beijing, China, 2010. (In Chinese)
40. Oktavianus, Y.; Chang, H.; Goldsworthy, H.M.; Gad, E.F. Component model for pull-out behaviour of headed anchored blind bolt within concrete filled circular hollow section. *Eng. Struct.* **2017**, *148*, 210–224. [[CrossRef](#)]
41. Su, Q.; Yang, G.; Bradford, M.A. Bearing Capacity of Perfobond Rib Shear Connectors in Composite Girder Bridges. *J. Bridg. Eng.* **2016**, *21*, 06015009. [[CrossRef](#)]
42. He, S.; Fang, Z.; Fang, Y.; Liu, M.; Liu, L.; Mosallam, A.S. Experimental study on perfobond strip connector in steel–concrete joints of hybrid bridges. *J. Constr. Steel Res.* **2016**, *118*, 169–179. [[CrossRef](#)]
43. Guo, Z.; Shi, X. *Theory and Analysis Of reinforced Concrete*; Tsinghua University Press: Beijing, China, 2003; pp. 163–337. (In Chinese)
44. GB 50017; Code for Design of Steel Structures. China Construction Industry Press: Beijing, China, 2017. (In Chinese)
45. *Code of Practice for the Structural Use of Steel 2011*; Buildings Department: Hong Kong, China, 2023.
46. JTG D64; Specifications for design of highway steel bridge. China Communications Press: Beijing, China, 2015. (In Chinese)

Disclaimer/Publisher’s Note: The statements, opinions and data contained in all publications are solely those of the individual author(s) and contributor(s) and not of MDPI and/or the editor(s). MDPI and/or the editor(s) disclaim responsibility for any injury to people or property resulting from any ideas, methods, instructions or products referred to in the content.